Research Article

Journal of PeptideScience

Received: 11 March 2010 Revised: 13 August 2010 Accepted: 10 September 2010 Published online in Wiley Online Library: 11 January 2011

(wileyonlinelibrary.com) DOI 10.1002/psc.1313

Analysis of the interacting surface of maurotoxin with the voltage-gated *Shaker* B K^+ channel

Ziad Fajloun,[a,b]* Nicolas Andreotti,[a] Mohamed Fathallah,[c] Jean-Marc Sabatier[a] and Michel De Waard[d]

Maurotoxin (MTX) is a 34-residue toxin that was isolated initially from the venom of the scorpion *Scorpio maurus* palmatus. Unlike the other toxins of the α-KTx6 family (Pi1, Pi4, Pi7, and HsTx1), MTX exhibits a unique disulfide bridge organization of the type C_1-C_5, C_2-C_6, C_3-C_4, and C_7-C_8 (instead of the conventional C_1-C_5, C_2-C_6, C_3-C_7, and C_4-C_8, herein referred to as Pi1-like) that does not prevent its folding along the classic α/β scaffold of scorpion toxins. MTX_{Pi1} is an MTX variant with a conventional pattern of disulfide bridging without any primary structure alteration of the toxin. Here, using MTX and/or MTX_{Pi1} as models, we investigated how the type of folding influences toxin recognition of the *Shaker* B potassium channel. Amino acid residues of MTX that were studied for *Shaker* B recognition were selected on the basis of their homologous position in charybdotoxin, a three disulfide-bridged scorpion toxin also active on this channel type. These residues favored either an MTX- or MTX_{Pi1}-like folding. Our data indicate clearly that Lys^{23} and Tyr^{32} (two out of ten amino acid residues studied) are the most important residues for *Shaker* B channel blockage by MTX. For activity on SKCa channels, the same amino acid residues also affect, directly or indirectly, the recognition of SK channels. The molecular modeling technique and computed docking indicate the existence of a correlation between the half cystine pairings of the mutated analogs and their activity on the *Shaker* B K^+ channel. Overall, mutations in MTX could, or could not, change the reorganization of disulfide bridges of this molecule without affecting its α/β scaffold. However, changing of the peptide backbone (cross linking disulfide bridges from MTX-like type *vs* MTX_{Pi1}-like type) appears to have less impact on the molecule activity than mutation of certain key amino acids such as Lys^{23} and Tyr^{32} in this toxin. Copyright © 2011 European Peptide Society and John Wiley & Sons, Ltd.

Keywords: Maurotoxin; *shaker* B K^+ channel; molecular modeling; computed docking; protein-protein interaction

Introduction

Maurotoxin (MTX) is a toxin isolated from the venom of the chactidae scorpion *Scorpio maurus* palmatus. It is a 34-mer peptide, cross-linked by four disulfide bridges, that is active on both voltage-gated (Kv) and calcium-activated (SK) potassium channel subtypes [1,2]. The solution structure of synthetic MTX has been solved by the ^{1}H-nuclear magnetic resonance (NMR) technique [3]. MTX is structured according to the 'classical' α/β scaffold reported to be present in most scorpion toxins studied hitherto independently of peptide length and pharmacology [4,5]. In the case of MTX, this structural motif is composed of a short α-helix (a combination of both 3.6_{13} and 3_{10} helix types) connected to a two-stranded β-sheet structure by two disulfide bridges [3]. This motif is reportedly associated with the presence of a consensus sequence of the type [. . .]C_1[. . .]C_2XXXC_3[. . .](G/A/S)XC_4[. . .]C_5XC_6[. . .] for three disulfide-bridged scorpion toxins active on K^+ channels [4,5]. This motif is also valid for four disulfide-bridged scorpion toxins active on Na^+ channels, with the two additional half-cystines located at each extremity of the peptide chain [6]. The connection between pairs of half-cystines that results from this motif is C_1-C_4, C_2-C_5 and C_3-C_6 or C_1-C_5, C_2-C_6, C_3-C_7 and C_4-C_8 for three or four disulfide-bridged toxins respectively. In the case of MTX, a modified motif, i.e. [. . .]C_1[. . .]C_2XXPC_3[. . .]C_4[. . .](A/S)XC_5[. . .]C_6XC_7[. . .]C_8, is observed in which one extra half-cystine (here C_4) is inserted in the central part of the motif, whereas the other (C_8) is located at the C-terminus of the peptide [1,2]. This structural variation is associated with an uncommon disulfide bridge organization of the type C_1-C_5, C_2-C_6, C_3-C_4, and C_7-C_8 in which the two last connections are rearranged. We have demonstrated in the past

* *Correspondence to: Ziad Fajloun, Centre Azm pour la Recherche en Biotechnologie et ses Applications, EDST, Université Libanaise, Rue El Mittein, Tripoli, Liban. E-mail: zfajloun@ul.edu.lb*

a *ERT 62, Faculté de Médecine Nord, 13916 Marseille Cedex 15, France*

b *Centre Azm pour la Recherche en Biotechnologie et ses Applications, EDST, Université Libanaise, Rue El Mittein, Tripoli, Liban*

c *CIC 9502, INSERM APHM, Hôpital Sainte-Marguerite, Boulevard Sainte-Marguerite, 13009 Marseille, France*

d *Laboratoire Canaux Calciques, Fonctions et Pathologies, INSERM U836, Grenoble Neuroscience Institute, Bâtiment Edmond. J. Safra 38042 Grenoble Cedex 09, France*

Abbreviations used: *Boc,* tert-*butyloxycarbonyl; Fmoc, N^{α}-fluorenylmethyloxycarbonyl; HPLC, high pressure liquid chromatography; HsTx1, Toxin 1 from the scorpion* Heterometrus spinnifer; *IC_{50}, 50% inhibitory concentration; MTX, Maurotoxin from the scorpion* Scorpio maurus *palmatus; MTX_{Pi1}, MTX variant with a conventional pattern of disulfide bridging type Pi1; NMR, nuclear magnetic resonance; Pi1, Toxin 1 from the scorpion* Pandinus imperator*; Pmc, pentamethylchroman; RMSD, root mean square deviation;* Shaker *B, a voltage-gated K^+ channel subtype from* Drosophilia Melanogaster*; t-Bu,* tert-*butyl; Trt: Trityl.*

Journal of PeptideScience

that modifying the disulfide bridge arrangement of MTX, without altering its primary structure, impacts the activity of the toxin on the *Shaker* B K^+ channel [7]. We succeeded in producing an MTX variant that adopts Pi1-like disulfide bridges of the conventional type, i.e. C_1-C_5, C_2-C_6, C_3-C_7, and C_4-C_8 type [7]. This MTX variant, referred to as MTX_{Pi1}, was obtained by the innovative strategy of solid-phase peptide synthesis based on a temporary chemical modification of the side chain of a trifunctional MTX amino acid residue (Tyr^{32}) expected to guide the type of toxin half-cystine pairings. MTX_{Pi1} blocks, effectively *Shaker* B K^+, outward currents with higher affinity than MTX [7]. Besides obtaining this analog through Tyr^{32} modification, we also observed that similar shifts in half-cystine pairings could be produced by introducing selected point mutations in MTX amino acid sequence [8–10]. The MTX_{Pi1} pattern is the native pattern of the MTX-related toxin, such as Pi1 [11] and HsTx1 [12], both short-chain four disulfide-bridged scorpion toxins sharing a high degree of sequence identity with MTX (from 53% to 68%). In spite of these differences in half-cystine pairings, these toxins still fold according to the α/β scaffold, which is assumed to represent a structural prerequisite for ion channel blocking activity. The maintenance of the α/β motif is, however, accompanied by small structural modifications, such as the relative orientation between the axis of the helix and the β-sheet structures, that impact the pharmacological affinity and/or selectivity toward their ion channel targets [8–10]. These variations in pharmacological profiles resulting from rearrangements of disulfide bridges are likely due to the spatial repositioning of some key amino acid residues that are involved in ion channel pore recognition.

In the present study, we took advantage of these earlier observations to further characterize how single amino acid substitution induces a Pi1-like disulfide bridge pattern of MTX and influences *Shaker* B recognition. To this aim, we selected ten residues of MTX on the basis of their homologous position in charybdotoxin, a three disulfide-bridged scorpion toxin whose interacting surface with *Shaker* B has been extensively investigated previously [13–15]. The molecular modeling technique and computed docking have been used to assess the structural impact of the amino acid substitutions on the disulfide bridge rearrangement (from MTX-type to Pi1-type) and on the interacting surface between MTX and the *Shaker* B K^+ channel. The data confirm that the conventional pattern is better suited than the atypical MTX pattern for *Shaker* B recognition.

Experimental Procedures

Materials

$N\alpha$–fluorenylmethyloxycarbonyl (Fmoc)-L-amino acids, Fmoc-amide resin, and reagents used for peptide synthesis were obtained from Perkin–Elmer Life Sciences. Solvents were analytical-grade products from SDS. Enzymes (trypsin, and chymotrypsin) were obtained from Roche Molecular Biochemicals.

Chemical Synthesis and Physicochemical Characterization of the MTX Analogs

The MTX analogs were obtained by the solid-phase technique [16] using an automated peptide synthesizer (Model 433A, Applied Biosystems Inc.). Peptide chains were assembled stepwise on 0.25 mc. of Fmoc-amide resin (1% cross-linked, 0.65 mequiv. of amino group/g) using 1 mmol of Fmoc-amino acid derivatives [17]. The side-chain-protecting groups used for trifunctional residues were as follows: trityl (Trt) for Cys, Asn, and Gln; *tert*-butyl (*t*-Bu) for Ser, Thr, Tyr, and Asp; pentamethylchroman (Pmc) for Arg, and *tert*-butyloxycarbonyl (Boc) for Lys. $N\alpha$–amino groups were deprotected by treatment with 18% and 20% (v/v) piperidine/*N*-methylpyrrolidone for 3 and 8 min respectively. The Fmoc-amino acid derivatives were washed several times with *N*-methylpyrrolidone (5 × 1 min) and coupled (20 min) as their hydroxybenzotriazole active esters (OBt) in *N*-methylpyrrolidone (fourfold excess). After peptide chain assemblies were completed and the N-terminal Fmoc groups removed, each peptide resin (from 1.5 to 2.0 g) was treated under stirring for 3 h at 20 °C with a mixture of trifluoroacetic acid/H_2O/thioanisole/ethanedithiol (88 : 5 : 5 : 2, v/v) in the presence of crystalline phenol (2.25 g) in a final volume of 30 ml/g of peptide resin. Each peptide mixture was then filtered to remove the resin, and the filtrates were precipitated and washed three times by adding cold *t*-butylmethyl ether. The resulting crude peptides were pelleted by centrifugation (3000 g; 10 min) and the supernatants were discarded. The peptides were dissolved in H_2O and freeze dried. The reduced peptides were then dissolved in 0.2 M tris/HCl buffer, pH 8.3, at final concentrations of 2 mM and stirred under air to allow folding/oxidation (72 h, 20 °C). The target products, MTX analogs, were purified to homogeneity by semipreparative reversed-phase high-pressure liquid chromatography (HPLC) (Perkin–Elmer, C_{18} Aquapore ODS 20 µm, 250 × 10 mm) by means of a 60-min linear gradient of 0.08% (v/v) trifluoroacetic acid (TFA)/0% to 40% acetonitrile in 0.1% (v/v) TFA/H_2O at a flow rate of 5 ml/min (λ = 230 nm). The homogeneity and identity of MTX analogs were assessed by (i) analytical C_{18} reversed-phase HPLC (Merck, C_{18} Lichrospher 5 µm, 4 × 200 mm) using a 60-min linear gradient of 0.08% (v/v) TFA/0% to 60% acetonitrile in 0.1% (v/v) TFA/H_2O at a flow rate of 1 ml/min; (ii) amino acid analysis after acidolysis (6 N HCl/2% (w/v) phenol, 20 h, 118 °C, under N_2); and (iii) mass spectrometry analysis.

Peptide Modeling and Molecular Mechanics Calculations

Steric energy calculations were used to determine which type of half-cystine pairing pattern (Pi1/HsTx1 type *versus* MTX type) was the most energetically favoured in the MTX analogs. These calculations were based on the three-dimensional (3D) structure of MTX obtained from the Protein Data Bank [3]. For point mutations, MTX amino acid residues were substituted by alanyl and full minimization was performed for each of the two types of disulfide pairing patterns. Minimization was achieved using the molecular modeling program Discover from the Insight II 98 package (Molecular Simulations Inc.), and the consistent valence force field (CVFF). The mathematical method used for minimization was the gradient conjugate. Multiple iterations were achieved for each analog until the root mean square derivative of the energy function was less than 0.001 kcal/mol.

Assignment of Half-Cystine Pairings of Synthetic MTX Analogs

The synthetic MTX analogs (100 µg for each peptide) were incubated with a mixture of trypsin and chymotrypsin at 10% (w/w) in 0.2 mM tris/HCl, pH 7.4, for 12 h at 37 °C. The peptide fragments purified by analytical reverse-phase HPLC (Merck, C_{18} Lichrospher 5 mm, 4 × 200 mm) with a 60-min linear gradient of 0.08% (v/v) trifluoroacetic acid/0% to 50% acetonitrile in 0.1% (v/v) trifluoroacetic acid/H_2O at a flow rate of 1 ml × min^{-1} (λ = 230 nm), and freeze-dried prior to their analyses. The peptide

fragments were hydrolyzed by acidolysis (6 ml HCl/phenol) and their amino acid contents were analyzed (Beckman, System 6300 amino-acid analyzer). The peptide fragments were further characterized by mass spectrometry analysis (RP-DE Voyager, Perseptive Biosystems).

Electrophysiological Recordings

Oocytes preparation

Xenopus laevis oocytes were isolated at stages V and VI and prepared for cRNA injection and electrophysiological recordings, as previously described [18]. Briefly, oocytes were prepared by removing the follicular cell layer by enzymatic treatment with 2 mg/ml collagenase IA (Sigma) in classical Barth's medium (in mM: 88 NaCl, 1 KCl, 0.82 $MgSO_4$, 0.33 $Ca(NO_3)_2$, 0.41 $CaCl_2$, 2.4 $NaHCO_3$, 15 *N*-2-hydroxyethylpiperazine-*N*′-ethanesulphonic acid (HEPES), pH 7.4 with NaOH). The *Shaker* B-encoding plasmid was linearized with *Sma*I and transcribed by means of the T7 mMessage mMachine kit (Ambion). The cRNA was stored frozen in H_2O at −80 °C at 1 μg/μl. The cells were micro-injected 1 day latter with 50 nl of 0.2 μg/μl *Shaker* B cRNA. To favor channel expression, cells were incubated at 16 °C into a defined nutrient oocyte medium [19] 2–6 days before current recordings.

Electrophysiology

Standard two-microelectrode techniques were used at room temperature (18–23 °C) to record oocyte currents. Both current and voltage electrodes were filled with 140 mM KCl and had resistances comprising between 0.5 and 1 MΩ. Currents were recorded using a voltage-clamp amplifier (GeneClamp 500, Axon Instruments, Foster City, CA) interfaced with a 16-bit AD/DA converter (Digidata 1200A, Axon Instruments) for acquisition and voltage protocol application. Current records were sampled at 10 kHz and low-pass-filtered at 2 kHz using an eight pole Bessel filter and stored on computer for subsequent analysis. The extracellular recording solution contained (in mM): 88 NaCl, 10 KCl, 2 $MgCl_2$, 0.5 $CaCl_2$, 0.5 niflumic acid, 5 HEPES, pH 7.4 (NaOH). Leak and capacitive currents were subtracted on-line by a P/4 protocol. Residual capacitive artifacts were blanked for display purposes. Toxin solutions were superfused in the recording chamber at a flow rate of 2 ml/min using a ValveBank4 apparatus (Automate Scientific Inc.). 0.1% bovine serum albumin was added to the recording and perfusion solutions to prevent toxin loss to the plastic chamber and tubules and nonspecific binding onto the cell. Data analysis was performed using pCLAMP 6.0.3 software (Axon Instruments, Foster City, CA). The results are presented as mean ± SEM.

Competition assay on rat brain synaptosomes

Rat brain synaptosomes (P2 fraction) were prepared according to Gray and Whittaker [20]. The protein content was assayed by a modified Lowry method. [^{125}I]-apamin (2000 Ci/mmol) was obtained as described [21]. Aliquots of 50 μl 0.1 nM [^{125}I]-apamin were added to 400 μl synaptosome suspensions (0.4 mg protein/ml). Samples were incubated for 1 h at 0 °C with 50 μl of one of a series of concentrations of each MTX analog (10^{-4} to 10^{-15} M) in 500 μl final volume. The incubation buffer was 25 mM tris/HCl, 10 mM KCl, pH 7.2. The samples were centrifuged and the resulting pellets were washed three times in 1 ml of the same buffer. Bound radioactivity was determined (Packard Crystal II). The values expressed are the means of triplicate experiments. Nonspecific binding, less than 10% of the total binding, was determined in the presence of an excess (10 nM) of unlabeled apamin.

Results and Discussion

Primary Structure of Maurotoxin and Comparison with Charybdotoxin: Rationale for the Design of New MTX Analogs

Charybdotoxin (CTX) has been extensively studied for its interaction with *Shaker* [13–15]. We therefore aimed at taking advantage of this knowledge to better understand the structural and functional impact of MTX amino acids mutated in our new analogs. Figure 1(A) illustrates the amino acid sequence of MTX and its Cys-based alignment with CTX. CTX exhibits an extended N-terminal domain as compared to MTX that forms the third strand of the β-sheet structure. The relative positions of the helical and the two-stranded β-sheet structures of toxins are shown. MTX normally adopts a peculiar C_1-C_5, C_2-C_6, C_3-C_4, and C_7-C_8 disulfide bridge arrangement (Figure 1(B), left). With targeted point mutations, the peptide may possibly adopt another type of disulfide bridging, C_1-C_5, C_2-C_6, C_3-C_7, and C_4-C_8, inasmuch as does Pi1 or HsTx1, two related toxins. This pattern is therefore referred to as the Pi1/HsTx1 pattern or MTX_{Pi1} pattern (Figure 1(B), right). In bold, we have highlighted the MTX amino acid residues that were mono-substituted by alanyl during production of the MTX analogs presented herein (Figure 1(A)). Two types of analogs were produced: first, analogs with mutations of residues unlikely to be involved directly in *Shaker* B recognition (Ala^2, Ala^4, Ala^6, Ala^7, Ala^{10}, Ala^{12}, Ala^{20}, and Ala^{33}); and, second, two analogs with mutations of residues directly implicated in the recognition of *Shaker* B (Ala^{23} and Ala^{32}). All analogs were designed with the aim to understand the involvement of the selected residues in the formation of the disulfide bridge pattern of MTX. All are amino acid residues, identical or similar to those of CTX, except Tyr^{10}, Pro^{12}, Pro^{20}, and Gly^{33}. The two Pro residues were chosen because of the structural constraints they induce in the MTX structure, suggesting that they were susceptible to influence MTX disulfide bridge pattern. As a matter of fact, the double mutation Ala^{12} and Ala^{20} was shown to produce the Pi1-like disulfide bridging [10]. Gly^{33} was chosen because of its strategic location between Cys^{31} and Cy^{34}, also suggesting its potential involvement in the formation of this peculiar disulfide bridge. Some of these analogs were reported in earlier studies (Ala^{12}, Ala^{20}, and Ala^{33}) [9,10]. A 3D structural comparison between MTX, MTX_{Pi1}, and CTX is shown in Figure 1(C). The positioning and arrangement of these disulfide bridges are partially conserved (green colour). The change in the pattern of the disulfide bridge of MTX was earlier shown to be associated with the reorientation in space of the side chains of various critical amino acids [7]. The point-mutated MTX analogs, indicated by bold residues in Figure 1(A), were chemically synthesized according to the stepwise solid-phase method [16]. After TFA-based cleavage of the peptide-resins, the crude MTX analogs were left at 25 °C for 72 h in classical alkaline buffer for folding/oxidation [22], purified to homogeneity and characterized by analytical C_{18} reversed-phase HPLC, amino acid analysis, and mass spectrometry. Figure 1(D) summarizes the experimental molecular masses of the MTX analogs that all agree with the deduced molecular masses.

Relative Positioning of Key CTX Residues Involved in Shaker B Channel Blockage and Comparison with the Positioning of Homologous MTX Residues

Although both CTX and MTX potently block *Shaker* K^+ channels, they do so with more distant affinities than those between MTX and MTX_{Pi1} [7,13]. If this is a correct finding, then we would expect that the orientation of critical residues for *Shaker* B recognition differ

Journal of PeptideScience

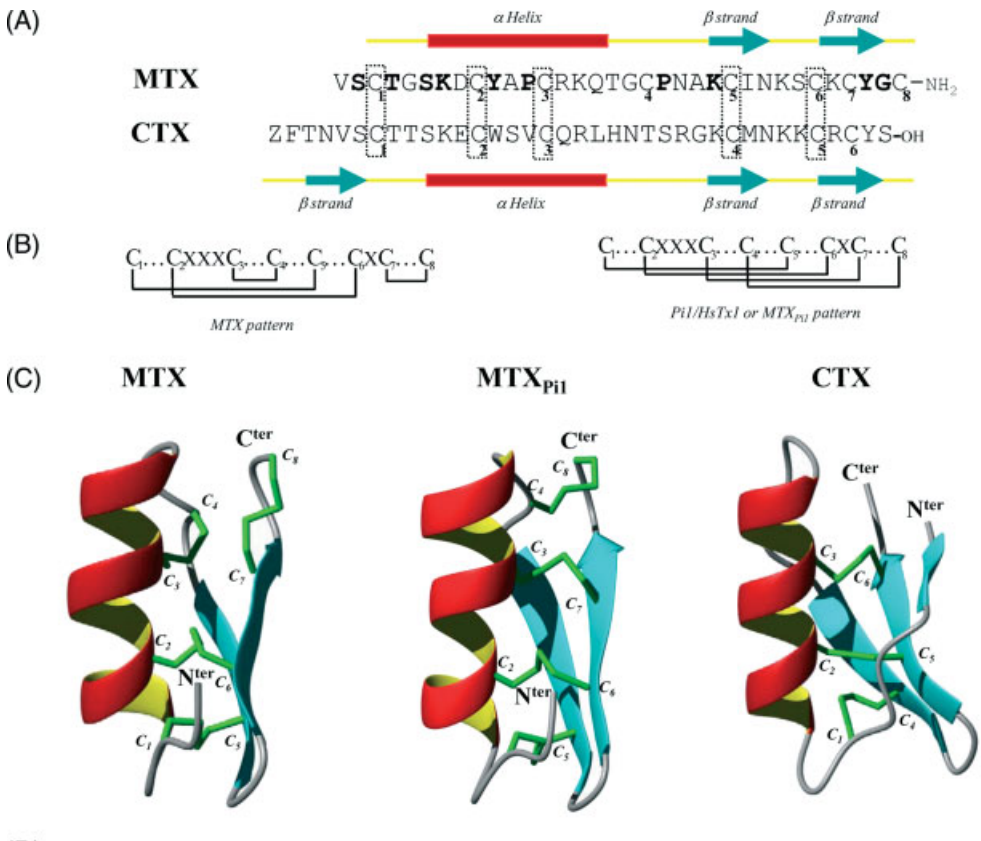

(D)

MTX analogues / Molecular Weight (Da)	[A²]MTX	[A⁴]MTX	[A⁶]MTX	[A⁷]MTX	[A¹⁰]MTX	[A¹²]MTX	[A²⁰]MTX	[A²³]MTX	[A³²]MTX	[A³³]MTX
Calculated	3604.25	3590.22	3604.25	3563.15	3528.15	3594.21	3594.21	3563.15	3528.15	3635.27
Experimental	3604.2	3590.4	3604.3	3563.1	3528.2	3594.2	3594.2	3563.1	3528.2	3635.3

Figure 1. (A) Comparison of MTX and CTX sequences (one-letter code). The half-cystine residues, critical to the 3D structures of peptides, are aligned and boxed. These residues are numbered by order of appearance from the N- to the C-terminus. The portions of the secondary structure of each toxin are mentioned according to the amino acid distribution in the sequence. The red bars match the α-helix portions and the blue arrows correspond to β-strands. Residues mutated to produce MTX analogs are in bold. (B) Assignment of the two patterns of disulfide bridging observed in MTX and Pi1/HsTX1 or MTX_{Pi1}. The disulfide bridges are depicted by plain lines. (C) Representation of the NMR 3D solution structure of MTX, MTX_{Pi1}, and CTX (from left to right, respectively). The α-helix, β-sheet, and disulfide bridges are highlighted in red, blue, and green respectively. The half-cystine residues are numbered as in parts (A and B). PDB codes are 1TXM (MTX) and 2CRD (CTX). (D) Different values of the deduced and experimental relative molecular masses of MTX and its synthetic structural analogs.

more between CTX and MTX than between MTX and MTX_{Pi1}. This information may be useful to determine what extent of variation is acceptable in lateral chain disposition for maintaining *Shaker* K^+ channel blockade. Key amino acid residues implicated in the recognition of *Shaker* B channels by CTX have been identified by extensive studies [23]. This information was used to draw a space-filling model of the 3D solution structure of CTX (Figure 2(A), left). These residues are Lys^{27} (shown in red in Figure 2), Met^{29}, Asn^{30}, Arg^{34}, and Tyr^{36}. According to the alignment of the toxin amino acid sequences presented in Figure 1(A), all of these CTX key residues have homologous residues in the MTX amino acid sequence. A similar space-filling model of MTX illustrates the positions of the equivalent amino acid residues (Figure 2(A), middle), i.e. Lys^{23} (Lys^{27} in CTX, shown in red in Figure 2), Ile^{25} (Met^{29} in CTX), Asn^{26} (Asn^{30} in CTX), Lys^{30} (Arg^{34} in CTX), and Tyr^{32} (Tyr^{36} in CTX). By molecular modeling, we also assessed the positions of these key amino acid residues for MTX_{Pi1} (Figure 2(A), right). Though the general feeling drawn from these space-filling models is that the relative positioning of these putative key residues are similar between CTX and MTX, or between MTX and MTX_{Pi1}, this representation is, however, quite inaccurate for a detailed inspection of residue side-chain orientation. We therefore looked for a more accurate representation of the spatial distribution of these amino acids. To this end, we superimposed the 3D functional maps of the three toxins to address the spatial distribution of key amino acid residues (Figure 2(B), left). This was achieved by using the best fit of the superimposition of two mean planes, each plane equally distributing the five key amino acid residues in space. This procedure yielded better mean RMSD values than those taking the central lysine (MTX or MTX_{Pi1} Lys^{23} or CTX Lys^{27}) as a common reference point. We next established the distances separating each of the α-carbon atoms of homologous

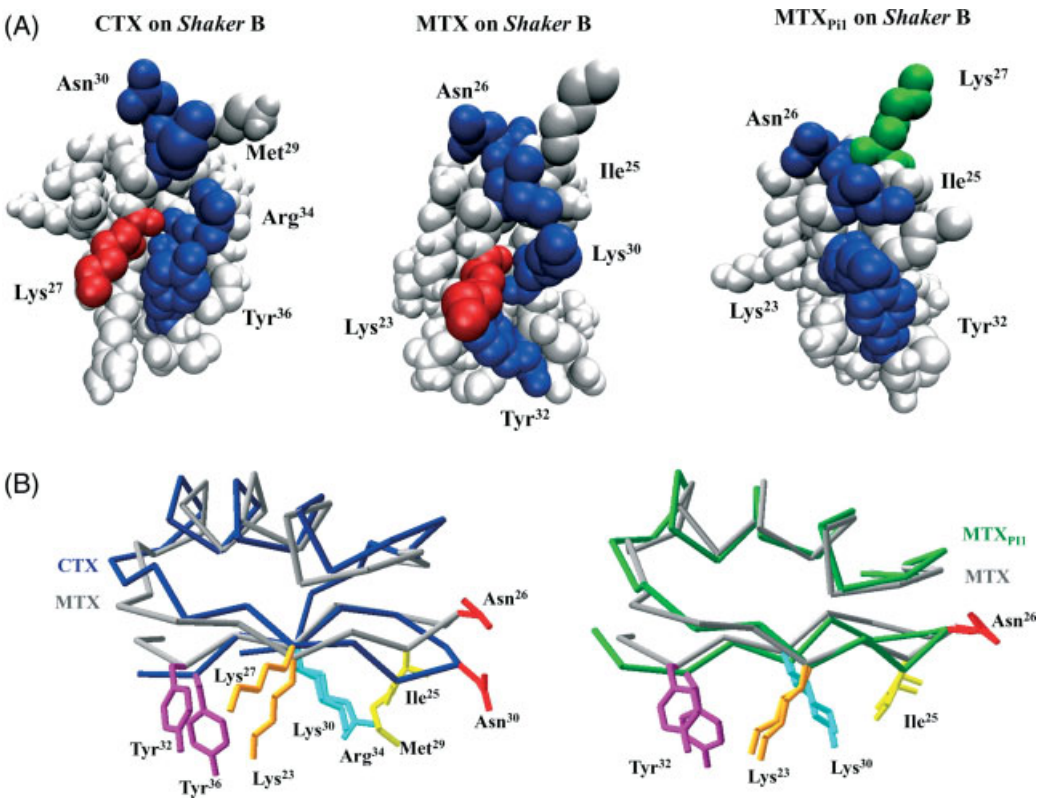

Figure 2. (A) Theoretical functional maps of CTX, MTX, and MTX$_{Pi1}$ (from left to right, respectively) that highlight key amino acid residues for peptide interaction with the *Shaker* B K^+ channel (dark blue residues). The most important residue Lys^{27} in CTX and Lys^{23} in MTX is shown in red. These residues are numbered according to the amino acid sequences. Lys^{27} of MTX$_{Pi1}$, interacting with Ser^{379} of *Shaker* B, is in green. The structures of scorpion toxins are shown according to a space-filling representation (TURBO-FRODO software). (B) *Left*: Superimposition of the 3D functional maps that address the spatial distribution of putative CTX and MTX key amino acid residues. *Right*: Superimposition of the 3D functional maps that address the spatial distribution of putative MTX and MTX$_{Pi1}$ key amino acid residues. The two representations were achieved by using the best fit of the superimposition of the two mean planes, each plane equally distributing the five key amino acid residues of MTX or CTX in space.

amino acid residues (Table 1). Regarding the comparison of MTX and CTX, we show that the RMSD values vary from 0.7 Å (MTX Lys^{23} to CTX Lys^{27}) to 2.06 Å (MTX Lys^{30} to CTX Arg^{34}). Some of the differences observed in the distance of the α-carbon atom are meaningless, however, as several key amino acid residues are not identical between CTX and MTX (MTX Ile^{25}/CTX Met^{29}, and MTX Lys^{30}/CTX Arg^{34}). The distances observed between the α-carbon atoms of MTX Ile^{25} and CTX Met^{29} (2.04 Å) and MTX Lys^{30} and CTX Arg^{34} (2.06 Å) may well be compensated by the length of the amino acid side-chain. This imperfect superimposition between the positions of the α-carbon atoms of homologous amino acid residues should explain the changes in the toxin affinity for *Shaker* B channels (120 nM for CTX *vs* 3 nM for MTX) [8,23]. In contrast, the difference in the toxin affinity for *Shaker* B channels is milder between MTX and MTX$_{Pi1}$ (3.4 nM for MTX *vs* 0.24 nM for MTX$_{Pi1}$) [7]. We therefore expected that with the MTX$_{Pi1}$ disulfide bridge pattern, we should obtain a better fit in the superimposition of the α-carbons of the key residues involved in *Shaker* B recognition between MTX and MTX$_{Pi1}$ than that with CTX. This was indeed observed, as shown in Figure 2(B) (right). The mean RMSD value was 1.05 Å, which was smaller than the one observed when MTX and CTX were compared (Figure 2(B), left). Individual RMSD values varied from 0.16 to 1.6 Å (Table 1). Though MTX is highly reticulated and presumably displays a greater rigidity than nonreticulated peptides, there is nevertheless a certain degree of flexibility in both the peptide backbone and residue side-chain positions. From the structural comparisons of MTX *versus* CTX, and MTX *versus* MTX$_{Pi1}$, one could tentatively assume that mean RMSD values equaling 1.05 Å induce more limited variations in the MTX binding affinity toward *Shaker* B channels than a mean RMSD variation of 1.69 Å. This mean RMSD value is used as a reference to better understand the structural and pharmacological changes that are observed with MTX analogs. The 14-fold difference in IC_{50} values for *Shaker* K^+ channels, observed experimentally for MTX$_{Pi1}$ and MTX, deserves some note because it can hardly be fully explained by such limited differences in RMSD values. In an earlier study, we had observed a greater number of molecular contacts of MTX$_{Pi1}$ with the *Shaker* B channel than those with MTX. For instance, Lys^{27} of MTX$_{Pi1}$ was found to interact with Ser^{379} of *Shaker* B [7], whereas Lys^{27} of MTX did not interact with any ion channel amino acid residue. This Lys^{27} residue is displayed in green in Figure 2(A) (right).

Effects of Point Mutations on the Disulfide Bridge Pattern (MTX-like or Pi1/HsTx1-like) of MTX Analogs

We next investigated the functional effects of selected MTX point mutations on peptide 3D structure, disulfide bridging, and pharmacology (competition assay with radiolabeled apamin for binding onto rat brain SK channels and blocking efficacy toward *Shaker* B K^+ currents). We focused on two types of single-point mutations corresponding to alanyl substitutions of either selected key residues implicated in the recognition of *Shaker* B or of residues lying outside the recognition surface. The latter

Journal of PeptideScience

Table 1. RMSD values for the comparison of CTX, MTX, MTX_{Pi1}, and MTX analogs

a. Comparison of various key residue variations of the RMSD MTX analogs with the corresponding ones according to scorpion toxin pattern MTX or Pi1/HsTX1 (all values in the table are in Å)

	A2	A4	A6	A7	A10	A12	A20	A23	A32	A33
Pattern	MTX	MTX	MTX	MTX	MTX	Pi1/HsTX	Pi1/HSTX	MTX	Pi1/HsTX	Pi1/HsTX
Overall mean RMSD	0.26	0.64	0.84	0.15	0.98	0.54	0.43	0.93	1.6	0.21
Lys^{23}	0.12	0.56	0.68	0.21	0.83	0.14	0.21	0.93	0.88	0.25
Ile^{25}	0.32	0.27	0.39	0.14	0.76	0.29	0.32	0.99	0.97	0.11
Asn^{26}	0.24	0.43	0.62	0.25	0.86	0.22	0.18	0.73	1.03	0.12
Lys^{30}	0.17	0.25	0.76	0.23	0.69	0.24	0.23	0.89	1.09	0.20
Tyr^{32}	0.28	0.55	0.84	0.16	0.92	0.29	0.21	0.79	1.12	0.19

b. RMSD variations between key residues of MTX *versus* CTX:

	Lys^{23}/Lys^{27}	Ile^{25}/Met^{29}	Asn^{26}/Asn^{30}	Lys^{30}/Arg^{34}	Tyr^{32}/Tyr^{36}
RMSD values	0.7	2.04	1.82	2.06	1.04

c. RMSD variations between key residues of MTX *versus* MTX_{Pi1}:

	Lys^{23}	Ile^{25}	Asn^{26}	Lys^{30}	Tyr^{32}
RMSD values	0.16	0.59	0.45	0.32	0.52

Table 2. Most favored disulfide bridging (MTX *vs* Pi1/HsTx1 pattern) of MTX analogs by molecular modeling and steric energy calculations

Peptide	Steric energy: MTX pattern (kcal/mol)	Steric energy: Pi1/HsTx1 pattern (kcal/mol)	Deduced pattern
MTX	885.6	912.0	MTX
$[A^2]$MTX	915.9	902.7	Pi1/MTX
$[A^4]$MTX	885.8	914.1	MTX
$[A^6]$MTX	882.7	907.0	MTX
$[A^7]$MTX	731.3	752.1	MTX
$[A^{10}]$MTX	865.7	907.8	MTX
$[A^{12}]$MTX	897.4	895.6	Pi1/HsTx1
$[A^{20}]$MTX	909.1	897.5	Pi1/HsTx1
$[A^{23}]$MTX	736.8	749.18	MTX
$[A^{32}]$MTX	914.3	901.6	Pi1/HsTx1
$[A^{33}]$MTX	921.8	905.2	Pi1/HsTx1

The Pi1/HsTx1 type of half-cystine pairings is associated with the lowest steric energy (most stable conformation) for $[A^2]$-MTX, $[A^{12}]$-MTX, $[A^{20}]$-MTX, $[A^{32}]$-MTX, and $[A^{33}]$-MTX.

mutations were interesting for three reasons: (i) they may or may not alter MTX recognition surface indirectly toward the *Shaker* B channel, (ii) they may impact the native disulfide bridging pattern of MTX, and (iii) finally they may help in defining MTX critical residues involved in SK channel recognition. Prior to assessing the effects of such alanyl substitutions on the spatial distribution of key residues of MTX and on peptide pharmacology, we first investigated, by computer-assisted molecular modeling and steric energy calculations, which disulfide bridge pattern, MTX *versus* Pi1/HsTx1 types, was the most energetically favored for all the MTX analogs. As shown in Table 2, the Pi1/HsTx1 half-cystine pairing type appears to be associated with the lowest steric energies (most stable conformations) for $[A^7]$-MTX, $[A^{12}]$-MTX, $[A^{20}]$-MTX, $[A^{32}]$-MTX, and $[A^{33}]$-MTX. Conversely, steric energies were found to converge minimally toward the MTX pattern for analogs that exhibited an experimental MTX disulfide bridging (analogs with a single mutation at position 2, 4, 6, 10, or 23). In the second step, all synthetic MTX analogs were proteolyzed by a mixture of trypsin and chymotrypsin and two or three decisive peptides of the resulting proteolytic fragments were characterized by amino acid analysis and mass spectrometry to address the half-cystine pairings of the synthetic analogs experimentally. The results of the enzyme treatment are summarized in Table 3. The disulfide bridge patterns determined for the different MTX analogs are in perfect agreement to those reported in combination with the steric energy values. These data suggest that the pattern of half-cystine pairings is tightly dictated by the nature of some key residues within MTX amino acid sequence. This has also been disclosed in our previous studies concerning synthetic MTX analogs [9].

Structural Impact and Pharmacological Effect of Point Mutations on the MTX Interacting Surface

By homology with amino acid residues, reportedly important for CTX-induced Shaker B blockage [12–14], we selected and produced two point-mutated MTX analogs, $[A^{23}]$-MTX and $[A^{32}]$-MTX, that predictably would present a reduced blocking efficacy on Shaker B channels. Figure 3(A) (left) indeed demonstrates that $[A^{23}]$-MTX and $[A^{32}]$-MTX block Shaker B currents with about 700- and >1000-fold reduction in affinity as compared to synthetic MTX, respectively. In Figure 3(A) (right), the calculated IC_{50}s for each of these peptides for Shaker B channels were 3.4 ± 1.9 nM (MTX), 3.1 ± 3.0 µM ($[A^{23}]$-MTX), and over 5 µM ($[A^{32}]$-MTX). At this peptide concentration, MTX almost fully blocks Shaker B currents, whereas no significant effect was detected on either the current amplitude or kinetic with the two MTX analogs. These data clearly indicate that Lys^{23} and Tyr^{32} are important residues for Shaker B channel blockage by MTX. They also suggest for the first time that MTX may block Shaker B channels through a CTX-resembling interacting surface. We have previously demonstrated that point

Table 3. Assignment of the half-cystine pairings by analyses of amino acid and mass spectrometry of two or three decisive peptide fragments for each MTX analog obtained by trypsin/chymotrypsin proteolysis (see section on 'Experimental Procedures') defining the different rearrangements of disulfide bridges

	Experimental Mr obtained (M+H$^+$)	Proteolytic Fragments identified	Half-cystinep airings determined
[A^2]-MTX Pi1/HsTx1pattern	1158.34	VACTGSK CINK	C_1-C_5
	1012.12	QTGCPNAK GC-NH2	C_4-C_8
[A^4]-MTX MTXpattern	1280.5	APCR QTGCPNAK	C_3-C_4
	478.50	CY GC-NH2	C_7-C_8
[A^6]-MTX MTXpattern	1158.35	VSCTGAK CINK	C_1-C_5
	1280.4	APCR QTGCPNAK	C_3-C_4
	478.45	CY GC-NH2	C_7-C_8
[A^7]-MTX MTXpattern	1117.2	VSCTGSA CINK	C_1-C_5
	1280.3	APCR QTGCPNAK	C_3-C_4
	478.45	CY GC-NH2	C_7-C_8
[A^{10}]-MTX MTXpattern	660.7	DCA SCK	C_2-C_6
	1280.5	APCR QTGCPNAK	C_3-C_4
[A1^2]-MTX Pi1/HsTx1pattern	720.8	AACR CY	C_3-C_7
	1012.11	QTGCPNAK GC-NH2	C_4-C_8
[A^{20}]-MTX Pi1/HsTx1pattern	987.0	QTGCANAK GC-NH2	C_3-C_4
	752.8	DCY SCK	C_2-C_6
[A^{23}]-MTX MTXpattern	1147.35	VSCTGSK CINK	C_1-C_5
	752.5	DCY SCK	C_3-C_4
	478.45	CY GC-NH2	C_7-C_8
[A^{32}]-MTX Pi1/HsTx1pattern	1147.3	VSCTGSK CINK	C_1-C_5
	752.85	DCYS CK	C_2-C_6
	1629.85	APCR QTGCPNAK CAGC-NH2	C_3-C_7/C_4-C_8
[A^{33}]-MTX Pi1/HsTx1pattern	1147.3	VSCTGSK CINK	C_1-C_5
	752.85	DCYS CK	C_2-C_6
	1026.10	QTGCPNAK AC-NH2	C_4-C_8

All the experimental masses obtained correspond perfectly to the deduced masses of proteolytic fragments.

mutations in MTX may result in a disulfide bridge rearrangement from the MTX pattern (C_1-C_5, C_2-C_6, C_3-C_4, and C_7-C_8) toward the Pi1/HsTx1 pattern (C_1-C_5, C_2-C_6, C_3-C_7, and C_4-C_8). This was predicted to be the case for [A^{32}]-MTX, but not for [A^{23}]-MTX (Tables 2 and 3). One could therefore wonder whether the pharmacological change resulting from the Tyr^{32} mutation is a consequence of the mutation per se or also results from disulfide bridge reorganization. However, the latter possibility appears unlikely as MTX mutations, known to impact the disulfide bridge organization (three disulfide-bridged MTX analog or Pi1/HsTx1-type bridging observed with [Q^{15}]-MTX, [A^{33}]-MTX, and MTX$_{Pi1}$), did not affect peptide pharmacology toward Shaker B channel [7–9]. Also, we observed that the mean RMSD value comparing the spatial distribution of key amino acid residues between MTX and MTX$_{Pi1}$ was quite low, a finding consistent with mean RMSD value variation for each individual key amino acid residue (Table 1). These considerations indicate that the relative positioning of MTX key amino acid residues involved – either directly or indirectly – in Shaker B channel recognition, may be slightly affected by the type of the pattern of the disulfide bridge. Figure 3(B) presents models

Journal of PeptideScience

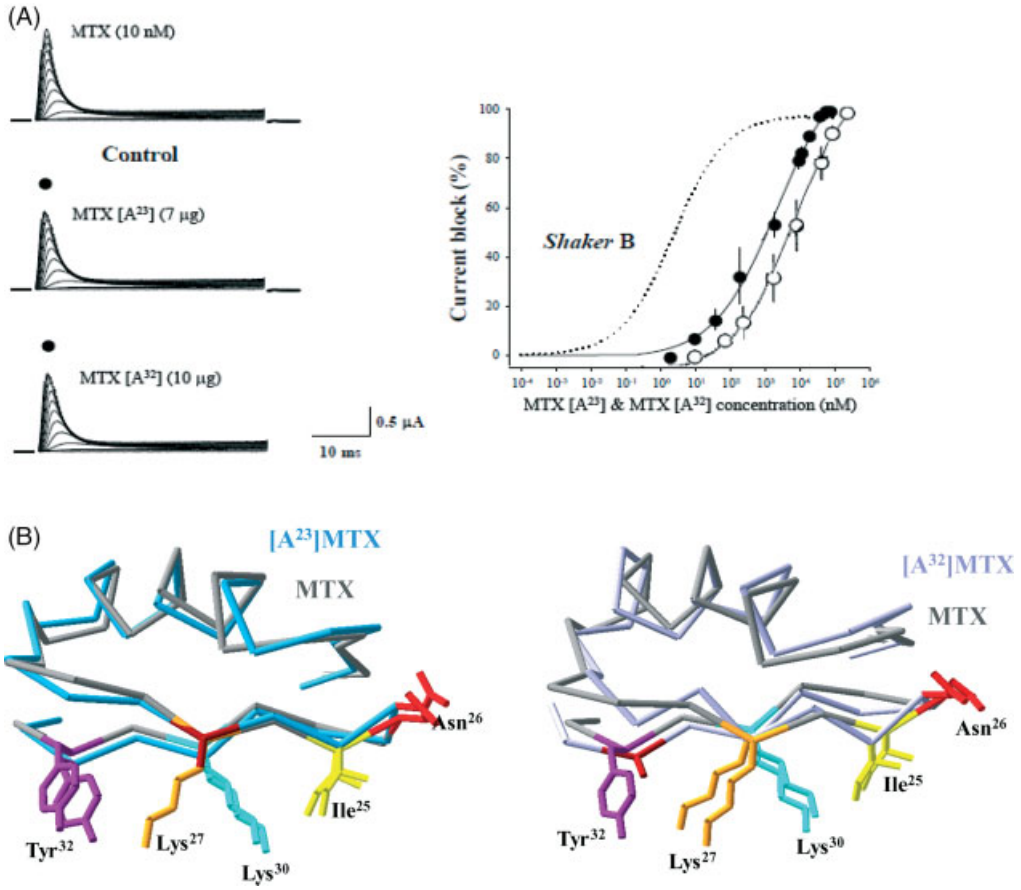

Figure 3. (A) MTX, [A^{23}]-MTX, and [A^{32}]-MTX are *Shaker* B K^+ channel blockers with different efficacies. *Left:* Oocytes expressing *Shaker* B K^+ currents recorded under two-electrode voltage clamp. *Right*: dose-dependent inhibition curves of *Shaker* B current by MTX (*dotted line)*, [A^{23}]-MTX (*filled circles*), and [A^{32}]-MTX (*open circles*). Data points are the mean ± S.E of $n = 6$. The *solid lines* through the data are from the equation $y = a/[1 + \exp(-(x - IC_{50})/b)]$ with IC_{50} values of 3.4 ± 1.9 nM (MTX), 3.1 ± 3.0 µM ([A^{23}]-MTX) and over 5 µM ([A^{32}]-MTX). (B) Superimposition of the 3D functional maps that address the spatial distribution of putative [A^{23}]-MTX and [A^{32}]-MTX key amino acid residues. The two representations were achieved by using the best fit of the superimposition of the two mean planes, each plane equally distributing the five key amino acid residues of MTX in space.

of [A^{23}]-MTX (with MTX disulfide bridging pattern) and [A^{32}]-MTX (with Pi1/HsTx1 disulfide bridging pattern). According to this representation, key amino acid residues of both analogs appear to be maintained in equivalent MTX-like positions. Superimposition of the α-carbons of [A^{23}]-MTX key amino acid residues (MTX disulfide bridging pattern, Tables 2 and 3) with that of MTX shows no significant deviation [mean RMSD value 0.93 Å, with slight individual variations, Figure 3(B), left]. This observation demonstrates that the pharmacological effect of Lys^{23} mutation is not associated with peptide backbone variation but with side-chain substitution in itself. These observations demonstrate that Lys^{23} is definitely required for Shaker B channel recognition. In contrast, mean RMSD value for [A^{32}]-MTX (Pi1/HsTx1 disulfide bridging pattern) is more marked (1.60 Å, Figure 3(B), right) than that for [A^{23}]-MTX. Also, stronger individual variations are observed in the case of this analog (Table 1). Whereas the mutation of Lys^{23} does not affect the spatial position of the α-carbon (RMSD 0.93 Å), the opposite is observed for the substitution of Tyr^{32} (RMSD 1.12 Å). Much less variation was observed in mean and individual RMSD values for [A^{32}]-MTX if one forces it to adopt an MTX-like disulfide bridging pattern (mean RMSD of 0.69 Å and individual RMSD for the Tyr^{32} substitution of 0.42 Å). Overall, the variation in RMSD values appears smaller than those observed for the comparison between MTX and CTX suggesting, again, that Tyr^{32} is also an important amino acid residue implicated in the recognition of Shaker B.

Identification of MTX Amino Acid Residues Implicated in SK Channel Binding

We tested the ability of the various MTX analogs to compete with [^{125}I]-apamin for binding onto rat brain synaptosomes. Table 4 illustrates the various IC_{50} values obtained for the inhibition of [^{125}I]-apamin binding. Unlabeled apamin itself produces a half-inhibition of [^{125}I]-apamin binding at a concentration of 2.8 ± 0.2 pM, whereas the IC_{50} value of MTX is 9.3 ± 0.3 nM; both values being in agreement with previous observations [8,9,24]. Significant changes were observed in the competition efficacies for several MTX analogs with the following rank orders (from the most to the least potent): MTX = [A^{10}]-MTX > [A^{2}]-MTX = [A^{7}]-MTX = [A^{4}]-MTX > [A^{33}]-MTX = [A^{6}]-MTX >> [A^{23}]-MTX = [A^{32}]-MTX. The reduction in competition efficacy thus ranged from 5- to over 7000-fold, depending on the MTX analog tested, except for [A^{10}]-MTX, which remained as potent as MTX. Several interesting conclusions can be raised from the comparison of the ability of the MTX analogs to compete with [^{125}I]-apamin for binding onto rat brain synaptosomes and their potencies to block *Shaker* B currents. First, it appears that amino acid residues that belong to the MTX surface implicated in the recognition of *Shaker* B (Lys^{23}

Table 4. Illustration of the various IC_{50} values obtained of the MTX and its synthetic structural analogs for inhibition of [^{125}I]-apamin binding

Peptides	Apamin	MTX	MTX_{Pi1}	[A^2] MTX	[A^4] MTX	[A^6] MTX	[A^7] MTX	[A^{10}] MTX	[A^{12}] MTX	[A^{20}] MTX	[A^{23}] MTX	[A^{32}] MTX	[A^{33}] MTX
Inhibition of [^{125}I] – apamin binding onto rat brain synaptosomes by apamin, MTX and MTX analogs													
$IC_{50} \pm$ S.D. (nM)	2.8 ± 0.2 pM	9.3 ± 0.3	17.4 ± 0.12	51 ± 10	74 ± 6	500 ± 180	65 ± 11	9 ± 2	N.D.	N.D.	38000± 33000	70, 000± 14, 000	395 ± 122
Shaker B current inhibition by MTX and MTX analogs													
$IC^{50} \pm$ S.D. (nM)	Inactive	3.4 ± 2.2	0.24 ± 1.2	5.3 ± 0.7	189 ± 375	∼1000	0.3 ± 0.3	>1000	1.1 ± 0.8	1.7 ± 1.1	3114 ± 3030	>10, 000	0.8 ± 0.3

Unlabeled apamin itself produces a half-inhibition of [^{125}I]-apamin binding at a concentration of 2.8 ± 0.2 pM, whereas the IC_{50} value of MTX is 9.3 ± 0.3 nM.

Journal of PeptideScience

and Tyr^{32}) may also affect, directly or indirectly, the recognition of SK channels. Indeed, individual alanyl substitution of these residues produce dramatic effects on both *Shaker* B currents and on [^{125}I]-apamin binding (reduction in efficacies comprised between 1000- and 10 000-fold). Beside these two residues, point mutation of Ser^6 by Ala also produced an MTX analog with diminished competition and blocking abilities, *ca* 50- to 300-fold. Second, the 'alanine scanning' method used in this study behaves as a powerful approach to obtain a number of MTX analogs exhibiting an increased selectivity for either *Shaker* B or SK channels. For instance, [A^7]-MTX was about tenfold more potent than MTX to block *Shaker* B currents, whereas it was sixfold less potent in competition assay with [^{125}I]-apamin. Conversely, [A^{10}]-MTX was as potent as MTX in the [^{125}I]-apamin binding assay, whereas its ability to block *Shaker* B currents was decreased by more than 200-fold. This MTX analog therefore appears to be unique as far in its ability to discriminate between SK and voltage-gated K^+ channels.

Conclusion

To date, the structures determined by NMR in solution for short-scorpion toxins acting on the K^+ channels appear to converge to a single overall α/β scaffold. It is therefore reasonable to expect that molecular modeling of these peptides produces reliable structural models that can be interpreted with regard to a given biological function. However, fine structural alterations (i.e. subtle changes in secondary structure elements and/or the relative orientation of side chains and/or the dynamic properties of the molecule) may be important for channel recognition. This point is illustrated by the present study. Analyses of the interaction surface of MTX and of its structural analogs with the *Shaker* B K^+ channel indicate that MTX_{Pi1} has a larger number of molecular contacts with the channel than MTX. MTX and MTX_{Pi1} have the same primary structure in common but differ only by their disulfide bridge organization. Thus, the spatial positioning of the side chain of certain key residues for the activity of short-scorpion toxins appears to be different in MTX with its native form (unconventional disulfide bridges) and in MTX_{Pi1} (conventional disulfide bridges). Overall, mutations in MTX could, or could not, change the reorganization of disulfide bridges of this molecule without affecting its α/β scaffold. Changing of the peptide backbone (cross-linking disulfide bridges) appears to have less impact on the molecule activity than mutation of certain key amino acids in this toxin. Our data will be helpful for a better understanding of the molecular determinants involved in recognition and interaction of short-scorpion toxin with K^+ channels. Besides, it should be useful to design new analogs with distinct structural and pharmacological properties.

References

1 Kharrat R, Mabrouk K, Crest M, Darbon H, Oughideni R, Martin-Eauclaire MF, Jacquet G, El Ayeb M, Van Rietschoten J, Rochat H, Sabatier JM. Chemical synthesis and characterization of maurotoxin, a short scorpion toxin with four disulfide bridges that acts on K^+ channels. *Eur. J. Biochem.* 1996; **242**: 491–498.

2 Kharrat R, Mansuelle P, Sampieri F, Crest M, Oughideni R, Van Rietschoten J, Martin-Eauclaire M-F, Rochat H, El Ayeb M. Maurotoxin, a four disulfide bridge toxin from *Scorpio maurus* venom: purification, structure and action on potassium channels. *FEBS Lett.* 1997; **406**: 284–290.

3 Blanc E, Sabatier J-M, Kharrat R, Meunier S, El Ayeb M, Van Rietschoten J, Darbon H. Solution structure of maurotoxin, a scorpion toxin from *Scorpio maurus*, with high affinity for voltage-gated potassium channels. *Proteins* 1997; **29**: 321–333.

4 Bontems F, Roumestand C, Gilquin B, Ménez A, Toma F. Refined structure of charybdotoxin : common motifs in scorpion toxins and insect defensins. *Science* 1991; **254**: 1521–1523.

5 Bonmatin JM, Bonnat JL, Gallet X, Vovelle F, Ptak M, Reichart JM, Hoffmann J, Keppi E, Legrain M, Achstetter T. Two-dimensional ^{1}H NMR study of recombinant insect defensin A in water: resonance assignments, secondary structure and global folding. *J. Biomol. NMR* 1992; **2**: 235–256.

6 Darbon H, Blanc E, Sabatier JM. Towards a new model of interaction of scorpion toxins with potassium channels. In *Perspectives in Drug Discovery and Design: Animal Toxins and Potassium Channels*, Vols. 15/16, Darbon H, Sabatier JM (eds). Kluwer Academic Publishers: Dordrecht, The Netherlands, 1999; 40–60.

7 M'Barek S, Lopez-Gonzalez I, Andreotti N, di Luccio E, Visan V, Grissmer S, Judge S, El Ayeb M, Darbon H, Rochat H, Sampieri F, Beraud E, Fajloun Z, De Waard M, Sabatier JM. A maurotoxin with constrained standard disulfide bridging: innovative strategy of chemical synthesis, pharmacology, and docking on K+ channels. *J. Biol. Chem.* 2003; **278**: 31095–31104.

8 Fajloun Z, Ferrat G, Carlier E, Fathallah M, Lecomte C, Sandoz G, di Luccio E, Mabrouk K, Legros C, Darbon H, Rochat H, Sabatier J-M, De Waard M. Synthesis, ^{1}H NMR structure, and activity of a three-disulfide-bridged maurotoxin analog designed to restore the consensus motif of scorpion toxins. *J. Biol. Chem.* 2000; **275**: 13605–13612.

9 Fajloun Z, Mosbah A, Carlier E, Mansuelle P, Sandoz G, Fathallah M, di Luccio E, Devaux C, Rochat H, Darbon H, De Waard M, Sabatier J-M. Maurotoxin *versus* Pi1/HsTx1 scorpion toxins: toward new insights in the understanding of their distinct disulfide bridge patterns. *J. Biol. Chem.* 2000; **275**: 39374–39402.

10 Carlier E, Fajloun Z, Mansuelle P, Fathallah M, Mosbah A, Oughideni R, Sandoz G, Di Luccio E, Geib S, Regaya I, Brocard J, Rochat H, Darbon H, Devaux C, Sabatier JM, De Waard M. Disulfide bridge reorganization induced by proline mutations in maurotoxin. *FEBS Lett.* 2001; **489**: 202–207.

11 Olamendi-Portugal T, Gomez-Lagunas F, Gurrola GB, Possani LD. A novel structural class of K^+-channel blocking toxin from the scorpion *Pandinus imperator*. *Biochem. J.* 1996; **315**: 977–981.

12 Lebrun B, Romi-Lebrun R, Martin-Eauclaire M-F, Yasuda A, Ishiguro M, Oyama Y, Pongs O, Nakajima T. A four-disulphide-bridged toxin, with high affinity towards voltage-gated K^+ channels, isolated from *Heterometrus spinnifer* (Scorpionidae) venom. *Biochem. J.* 1997; **328**: 321–327.

13 Naranjo D, Miller C. A strongly interacting pair of residues on the contact surface of charybdotoxin and the *Shaker* K^+ channel. *Neuron* 1996; **16**: 123–130.

14 Goldstein SA, Pheasant DJ, Miller C. The charybdotoxin receptor of a Shaker K^+ channel : peptide and channel residues mediating molecular recognition. *Neuron* 1994; **12**: 1377–1388.

15 Stampe P, Kolmakova-Partensky L, Miller C. Mapping hydrophobic residues of the interacting surface of charybdotoxin. *Biophys. J.* 1992; **62**: 8–9.

16 Merrifield RB. Solid phase synthesis. *Science* 1986; **232**: 341–347.

17 Sabatier JM. In *Handbook of Toxinology, Animal Toxins: Tools in Cell Biology*, Rochat H, Martin-Eauclaire MF (eds). Birkhäuser Verlag: Basel, Switzerland, 1999; 198–218.

18 De Waard M, Campbell KP. Subunit regulation of the neuronal α_{1A} Ca^{2+} channel. *J. Physiol.* 1995; **485**: 619–634.

19 Eppig JJ, Dumont JN. Defined nutrient medium for the *in vitro* maintenance of *Xenopus laevis* oocytes. *In Vitro* 1976; **12**: 418–427.

20 Gray EG, Whittaker VP. The isolation of nerve endings from brain: an electron microscopic study of cell fragments derived by homogenization centrifugation. *J. Anat.* 1962; **96**: 79–88.

21 Seagar M, Granier C, Couraud F. Interactions of the neurotoxin apamin with a Ca^{2+}-activated K^+ channel in primary neuronal cultures. *J. Biol. Chem.* 1984; **259**: 1491–1495.

22 Di Luccio E, Azulay DO, Regaya I, Fajloun Z, Sandoz G, Mansuelle P, Kharrat R, Fathallah M, Carrega L, Estève E, Rochat H, De Waard M, Sabatier JM. Parameters affecting *in vitro* oxidation/folding of maurotoxin, a four-disulphide-bridged scorpion toxin. *Biochem. J.* 2001; **358**: 681–692.

23 Possani LD, Selisko B, Gurrola GB. Structure and function of scorpion toxins affecting K^+ channels. In *Perspectives in Drug Discovery and Design: Animal Toxins and Potassium Channels*, Vols. 15/16, Darbon H, Sabatier JM (eds). Kluwer Academic Publishers: Dordrecht, The Netherlands, 1999; 15–40.

24 Lecomte C, Ferrat G, Fajloun Z, Van Rietschoten J, Rochat H, Martin-Eauclaire MF, Darbon H, Sabatier JM. Chemical synthesis and structure-activity relationships of Ts kappa, a novel scorpion toxin acting on apamin-sensitive SK channel. *J. Pept. Res.* 1999; **54**: 369–376.

